AMERICAN SOCIETY FOR MICROBIOLOGY | Journal of Virology®

VIRUS-CELL INTERACTIONS

Invasion of Herpes Simplex Virus 1 into Murine Dermis: Role of Nectin-1 and Herpesvirus Entry Mediator as Cellular Receptors during Aging

Lisa Wirtz,[a] Maureen Möckel,[a] Dagmar Knebel-Mörsdorf[a,b]

[a]Center for Biochemistry, University Hospital Cologne, University of Cologne, Cologne, Germany
[b]Department of Pediatrics, Faculty of Medicine, University Hospital Cologne, University of Cologne, Cologne, Germany

ABSTRACT Skin is a major target tissue of herpes simplex virus 1 (HSV-1), and we are only beginning to understand how individual receptors contribute to the initiation of infection in tissue. We recently demonstrated the impact of the receptors nectin-1 and herpesvirus entry mediator (HVEM) for entry of HSV-1 into murine epidermis. Here, we focus on viral invasion into the dermis, a further critical target tissue *in vivo*. In principle, murine dermal fibroblasts are highly susceptible to HSV-1, and we previously showed that nectin-1 and HVEM can act as alternative receptors. To characterize their contribution as receptors in dermal tissue, we established an *ex vivo* infection assay of murine dermis. Only after separation of the epidermis from the dermis, we observed single infected cells in the upper dermis from juvenile mice at 5 h postinfection with increasing numbers of infected cells at later times. While nectin-1-expressing cells were less frequently detected, we found HVEM expressed on most cells of juvenile dermis. The comparison of infection efficiency during aging revealed a strong delay in the onset of infection in the dermis from aged mice. This observation correlated with a decrease in nectin-1-expressing fibroblasts during aging while the number of HVEM-expressing cells remained stable. Accordingly, aged nectin-1-deficient dermis was less susceptible to HSV-1 than the dermis from control mice. Thus, we conclude that the reduced availability of nectin-1 in aged dermis is a key contributor to a decrease in infection efficiency during aging.

IMPORTANCE HSV-1 is a prevalent human pathogen which invades skin and mucocutaneous linings. So far, the underlying mechanisms of how the virus invades tissue, reaches its receptors, and initiates infection are still unresolved. To unravel the mechanical prerequisites that limit or favor viral invasion into tissue, we need to understand the contribution of the receptors that are involved in viral internalization. Here, we investigated the invasion process into murine dermis with the focus on receptor availability and found that infection efficiency decreases in aging mice. Based on studies of the expression of the receptors nectin-1 and HVEM, we suggest that the decreasing number of nectin-1-expressing fibroblasts leads to a delayed onset of infection in the dermis from aged compared to juvenile mice. Our results imply that the level of infection efficiency in murine dermis is closely linked to the availability of the receptor nectin-1 and can change during aging.

KEYWORDS HSV-1, HVEM, dermal fibroblasts, *ex vivo* infection, murine dermis, nectin-1, viral entry

During primary infection, herpes simplex virus 1 (HSV-1) enters its human host via mucosal surfaces, skin, or cornea, which is followed by latent infection of the peripheral nervous system. After penetration of the tissue, virus entry into individual cells requires the interaction of several virion envelope glycoproteins with various cell

Citation Wirtz L, Möckel M, Knebel-Mörsdorf D. 2020. Invasion of herpes simplex virus 1 into murine dermis: role of nectin-1 and herpesvirus entry mediator as cellular receptors during aging. J Virol 94:e02046-19. https://doi.org/10.1128/JVI.02046-19.

Editor Rozanne M. Sandri-Goldin, University of California, Irvine

Address correspondence to Dagmar Knebel-Mörsdorf, dagmar.moersdorf@uni-koeln.de.

Received 5 December 2019
Accepted 5 December 2019
Accepted manuscript posted online 11 December 2019
Published 14 February 2020

surface receptors (1). In principle, HSV-1 can attach to heparan sulfate side chains of cell surface proteoglycans (2, 3), which precedes the binding of the viral glycoprotein D (gD) to a receptor, leading to fusion with a cellular membrane (4, 5). The primary gD receptors for HSV-1 on murine and human cells are the cell-cell adhesion molecule nectin-1 and herpesvirus entry mediator (HVEM), a member of the tumor necrosis receptor superfamily (6, 7). Interactions of gD with nectin-1 and HVEM have been well studied in various cultured cells; however, we know less about their relevance for virus entry into tissue and under which conditions the receptors are accessible.

To investigate the viral invasion process into skin and to characterize the contributing receptors, we recently established an *ex vivo* infection model of murine epidermal sheets (8, 9). Intact murine skin samples are protected against invasion of HSV-1, indicating that the virus cannot penetrate via the apical surface of the epidermis. Even at the edges of the skin samples, infected keratinocytes are not detectable as long as the integrity of the tissue is maintained. However, when the dermis is removed from murine skin samples, epidermal sheets are highly susceptible to HSV-1 infection via the basal keratinocyte layer (8, 10). *Ex vivo* infection studies in HVEM- or nectin-1-deficient epidermis identified nectin-1 as the major receptor in murine epidermal sheets, while HVEM had a more limited role (10). These results are in line with the finding that HVEM is not the primary entry receptor in murine cornea but contributes to ocular HSV-1 pathogenesis, supporting entry-independent contributions of HVEM (11, 12).

During penetration via abraded skin (13) and upon viral reactivation, during which HSV-1 can be released from nerve endings within the dermal tissue, the dermis represents a further important target tissue *in vivo*. Thus, we previously addressed the contribution of nectin-1 and HVEM as receptors in dermal fibroblasts, which are the major resident cell type of the dermis. Murine primary dermal fibroblasts are highly susceptible to HSV-1 as long as one of the receptors is present, although nectin-1 acts as the more efficient receptor. In fibroblasts that are deficient in both receptors, infection is strongly reduced, supporting that nectin-1 and HVEM serve as alternative and major receptors (14). Here, we addressed the HSV-1 susceptibility of murine fibroblasts embedded in the dermis with the focus on receptor accessibility and distribution during aging. The dermis is composed of two distinct zones, which are largely based on their differences in connective tissue organization and cell density (15, 16). The papillary dermis, which is the closest to the epidermis and usually no more than twice its thickness, contains thin collagen fibrils and a high density of fibroblasts. The deeper dermis contains the reticular dermis with large collagen fibrils, which makes up the bulk of the dermis (Fig. 1A). As the composition and stiffness of the dermis change during aging, the tissue permeability might vary, which could contribute to the accessibility of the cells and thus to the efficiency of viral invasion. After we established an *ex vivo* infection assay to visualize HSV-1 entry into the dermis, we investigated whether the efficiency of entry differs in the dermis from young and aged mice. Interestingly, we found delayed infection efficiency in the dermis from aged mice. Strikingly, this finding correlated with decreased nectin-1 expression during aging, while levels of HVEM, which was expressed on most cells in the dermis, were unchanged. Thus, our conclusion is that delayed infection efficiency during aging is related to a drop of nectin-1 expression in the dermis from aged mice.

RESULTS

Infection of murine dermis with HSV-1. To address the susceptibility of the murine dermis to HSV-1, we first *ex vivo* infected the intact back skin of newborn mice. Viral transcripts were not detected even at 24 h postinfection (p.i.), indicating that neither the keratinocytes in the epidermis nor the fibroblasts in the dermis were infected (Fig. 1B). Our previous studies demonstrated that HSV-1 enters keratinocytes only after *ex vivo* infection of epidermal sheets (8, 10). Here, we confirmed by reverse transcriptase PCR (RT-PCR) that early viral transcripts such as the infected cell protein 0 (ICP0) and gD were present at 3 h after *ex vivo* infection of epidermal sheets (Fig. 1B). As a control for the susceptibility of murine dermal fibroblasts, we performed time course experiments

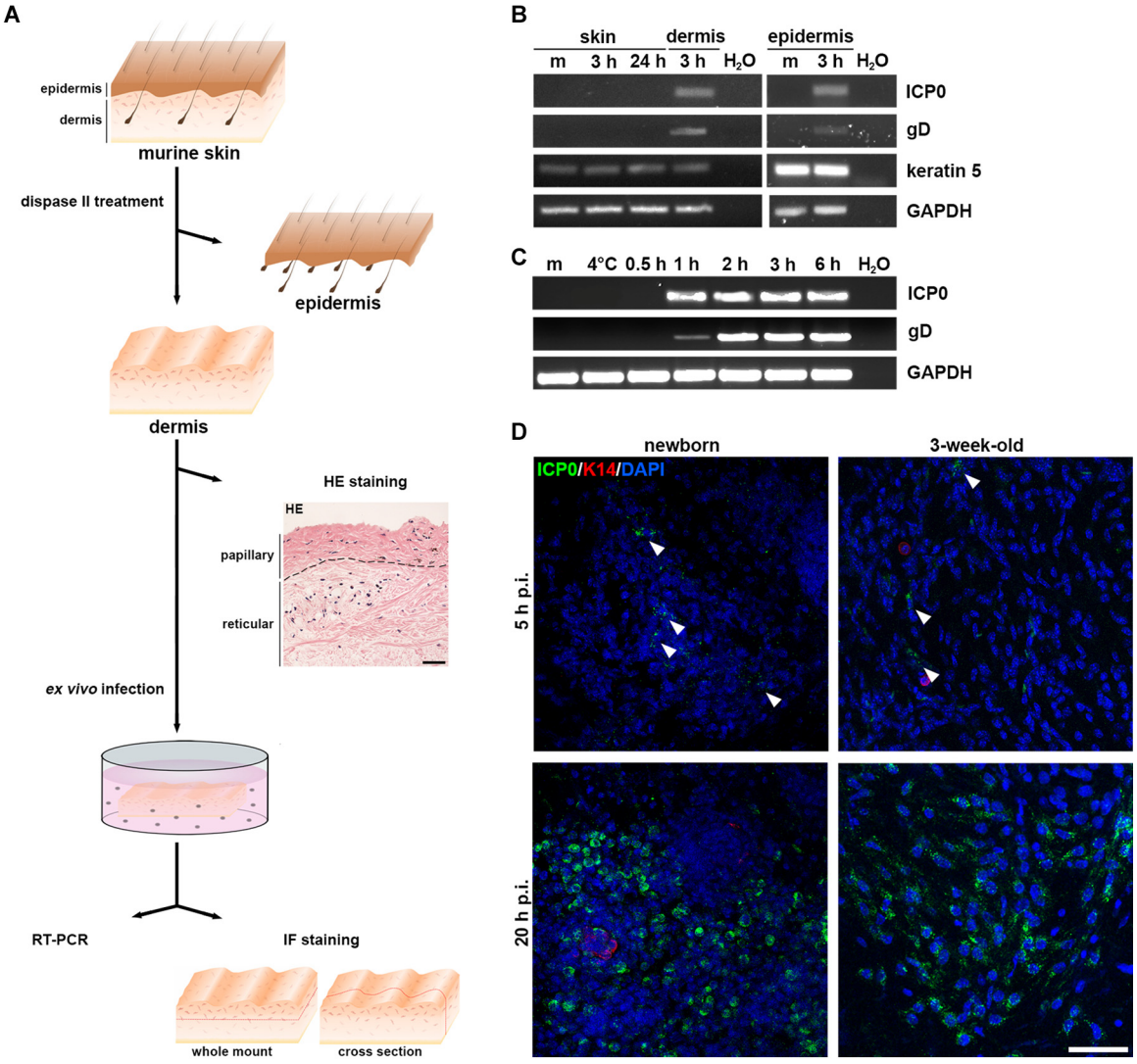

FIG 1 *Ex vivo* infection of murine dermis with HSV-1. (A) Schematic illustrating the preparation of murine dermal sheets followed by *ex vivo* infection. Hematoxylin and eosin (H&E)-stained section of the dermis from juvenile mouse tail visualizes the papillary and reticular layers. Scale bar, 25 μm. Immunofluorescence (IF) stainings of horizontal whole mounts show the distribution of infected cells in the apical layer of the papillary dermis, while stainings of vertical cross sections visualize infected cells throughout the dermis. (B) After infection with HSV-1 at a multiplicity of infection (MOI) of 50 PFU/cell, representative RT-PCR ($n = 3$) demonstrates the viral transcripts ICP0 and gD at 3 h p.i. in dermis and epidermis, which were prepared from newborn back skin. No viral RNAs were visible in the infected back skin of newborn mice at 24 h p.i. As a control, the presence of keratin 5 and GAPDH is shown. (C) Primary murine dermal fibroblasts were infected at 5 PFU/cell. ICP0 and gD transcripts were detected at 1 h p.i. Results ($n = 3$) are shown at the indicated h p.i. Infection for 1 h at 4°C served as a control (4°C). m, mock infected. (D) Dermal sheets from newborn and 3-week-old mice were infected at 50 PFU/cell. Immunostainings of whole mounts demonstrate ICP0-expressing cells (green) (arrowhead) at 5 h p.i. with increasing numbers at 20 h p.i. Confocal projections and merged images from at least 3 independent experiments show ICP0 (green) mainly in the cytoplasm, DAPI (blue) as the nuclear counterstain, and keratin 14 (red) to exclude infected keratinocytes. Scale bar, 50 μm.

and demonstrated the presence of viral transcripts already at 1 h p.i. (Fig. 1C). To allow enhanced viral access to the dermis, we separated the dermis from the epidermis by dispase II treatment prior to *ex vivo* infection (Fig. 1A). At 3 h p.i., we observed ICP0 and gD transcripts, indicating that HSV-1 can gain access to cells embedded in the dermis (Fig. 1B). However, preparations of dermal sheets might also contain keratinocytes, as epidermal appendages such as hair follicles span the dermis and are only partly removed after separation of the dermis from the epidermis. As we detected keratin 5 transcripts, we assumed that the viral transcripts could result from infection of both fibroblasts and keratinocytes in the newborn dermis (Fig. 1B).

To distinguish the infected cells in the dermis, we had to visualize them and thus established a protocol for preparing, sectioning, and immunostaining tissue samples

(Fig. 1A). We determined successful virus entry into individual cells in the dermis by visualizing ICP0. Once the viral genome is released into the nucleus, ICP0 first localizes in nuclear foci and then relocalizes to the cytoplasm during later infection (17, 18). Upon infection of newborn dermis with 50 PFU/cell, immunostainings visualized ICP0 at various times p.i. Only at 5 h p.i., dermal whole mounts showed some infected cells in the upper layer of the papillary dermis, with increasingly infected areas at 20 h p.i. (Fig. 1A and D). Infection of keratinocytes from the remaining hair follicles was excluded by counterstaining keratin 14 (Fig. 1D). Thus, we conclude that HSV-1 can indeed reach fibroblasts in the upper part of the papillary dermis from newborn mice once the epidermis is removed from the dermis.

As compared to juvenile mice, the dermal sheets from newborn mice are rather fragile, which might facilitate viral penetration. Thus, we also *ex vivo* infected the dermis from the tail skin of juvenile (3-week-old) mice. Tail skin was preferred because it harbors fewer hair follicles than back skin. While some infected cells were observed at 5 h p.i., most cells of the apical papillary dermis were infected at 20 h p.i. (Fig. 1D). These results indicate comparable infection efficiency of the dermis from newborn back skin and juvenile tail skin, suggesting that the mechanical differences of newborn and young dermis have no major influence on the accessibility of the receptors to initiate infection.

Entry of HSV-1 into collagen-embedded fibroblasts. In comparison to epidermal sheets, where nearly all cells of the basal layer expressed ICP0 at 3 h p.i. (10), the onset of infection in the fibroblasts of the dermis was strongly delayed. Evidently, the accessibility of the cells and receptors is completely different. While the epidermis is characterized by tight layers of differentiating keratinocytes, the dermis is composed of the extracellular matrix (ECM), in which fibroblasts of varying densities are embedded. To directly address the potential barrier function of the ECM and its impact on delayed infection, we used three-dimensional (3D) collagen I matrices in which dermal fibroblasts were embedded, allowing infection studies in a tissue-like environment (19). Collagen type I is the most abundant component of fibrous connective tissue, and fibroblasts are mainly responsible for collagen biosynthesis and remodeling. When fibroblasts are cultured in floating collagen I matrices, they cause matrix contraction that directly depends on the cell density and inversely on the collagen concentration, thus resembling a dermis-like structure (20, 21). To investigate the role of collagen I fibrils on infection efficiency of HSV-1 in a dermal equivalent, we embedded primary murine fibroblasts from newborn mice in increasing concentrations of collagen I. The lower the collagen I concentration was, the better the 3D gels were contracted, resulting in smaller gels than at higher collagen I concentrations (Fig. 2A). Upon infection of the smallest gel with the low collagen concentration of 0.3 mg/ml, we observed viral gD transcripts already at 3 h p.i. (Fig. 2B). In comparison, upon infection of primary dermal fibroblasts, gD RNA was detected at 1 h p.i. (Fig. 1C). With increasing concentrations of collagen, viral transcription was delayed but still detected at 6 h p.i. (Fig. 2B). These results imply that the density of collagen I fibrils has the potential to delay infection by most likely interfering with the accessibility of the cells.

Infection of murine dermis with HSV-1 during aging. Due to intrinsic (chronological) and extrinsic aging (photoaging) of skin, the mechanical properties of the dermis change, which is largely attributed to thinning of the tissue due to changes in the ECM and partial loss of ECM components (22–24). To address whether age-related changes influence the accessibility of the receptors, which, in turn, may result in changes in infection efficiency, we performed *ex vivo* infection studies of dermal sheets from aging mice. Our hypothesis was that thinning, increased fragility, and loss of elasticity might enhance accessibility of the receptors, which, in turn, would increase the viral susceptibility of the dermis.

When we *ex vivo* infected dermal sheets of 6- and 12-month-old mice, we observed no infected cells at 5 h p.i., while some infected cells were readily detected in 3-week-old dermis (Fig. 3A). At 16 h p.i., a nearly comparable number of infected cells

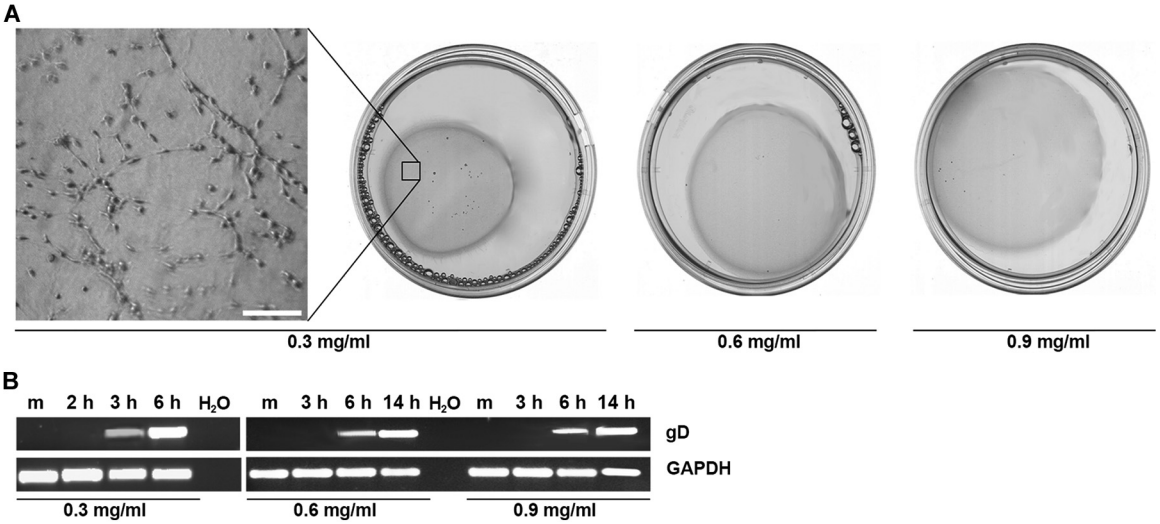

FIG 2 HSV-1 infection of fibroblasts embedded in floating collagen matrices. (A) Floating collagen matrices are shown at 5 h after seeding of murine dermal fibroblasts (1×10^6 cells) at varying collagen I concentrations. The magnification demonstrates fibroblasts embedded in collagen I (0.3 mg/ml). Scale bar, 300 μm. (B) At 5 h after seeding, the cells were infected with HSV-1 at 50 PFU/cell. RT-PCR ($n = 3$) indicates viral gD transcripts at 3 h p.i. in the lowest collagen concentration and at 6 h p.i. in higher collagen concentrations. m, mock infected.

was found in the papillary dermis of 3-week- and 6-month-old mice, demonstrating only a minor delay of virus entry in the adult compared to the juvenile dermis (Fig. 3A). In contrast, no infection was detected in 12-month-old dermis at 16 h p.i. (Fig. 3A). Only at 24 h p.i., some infected cells were evident, indicating a major delay of infection onset in aged dermis (Fig. 3A). Even at 48 h p.i., only some increase in the number of infected cells was visible (Fig. 3A). However, we observed ICP0 expression in most of the apical cells in the papillary dermis of 3-week- and 6-month-old mice already at 24 h p.i. (Fig. 3A). At this time, transmission light microscopy implies no major cytopathic effects in the tissue at all three ages (Fig. 3B).

As a control for tissue integrity after long incubation times, we incubated juvenile dermis for 48 h in the medium without observing any tissue damage in hematoxylin and eosin stain (H&E) stainings (Fig. 4A). In addition, terminal deoxynucleotidyltransferase-mediated dUTP-biotin nick end labeling (TUNEL) stainings confirmed the viability of nearly all cells in both juvenile and aged dermis at 5 and 48 h p.i. as well as after incubation in the medium for 48 h (Fig. 4B).

Taken together, our infection studies visualized that at least the papillary dermis is susceptible to HSV-1 in young and aged mice. However, there was some delay of infection in the 6-month-old dermis, which was much more pronounced in 12-month-old mice, suggesting that susceptibility to HSV-1 does not increase but rather decreases during aging.

Expression of nectin-1 and HVEM in the dermis of aging mice. To explore whether the reduced infection efficiency during aging correlates with changes in the expression level of the receptors nectin-1 and HVEM, we first performed RT-PCR. Unexpectedly, nearly no nectin-1 transcripts were detected in 6- and 12-month-old dermis in whom infection was delayed, while strong nectin-1 signals were evident in juvenile dermis, correlating with the most efficient infection (Fig. 3C). In addition, we detected only weak HVEM signals in 6- and 12-month-old dermis but strong signals in juvenile dermis (Fig. 3C). We then investigated cell surface expression of nectin-1 and HVEM by use of flow cytometry. As control experiments indicated that ca. 6% of the dermal cells represent macrophages (data not shown), we assumed that our flow cytometric analyses included mainly fibroblasts. After dissociation of dermal sheets from 3-week-, 6-month-, or 12-month-old mice, the HVEM-expressing population represented ca. 76, 74, and 64% of the analyzed cells, respectively (Fig. 5A). Comparable

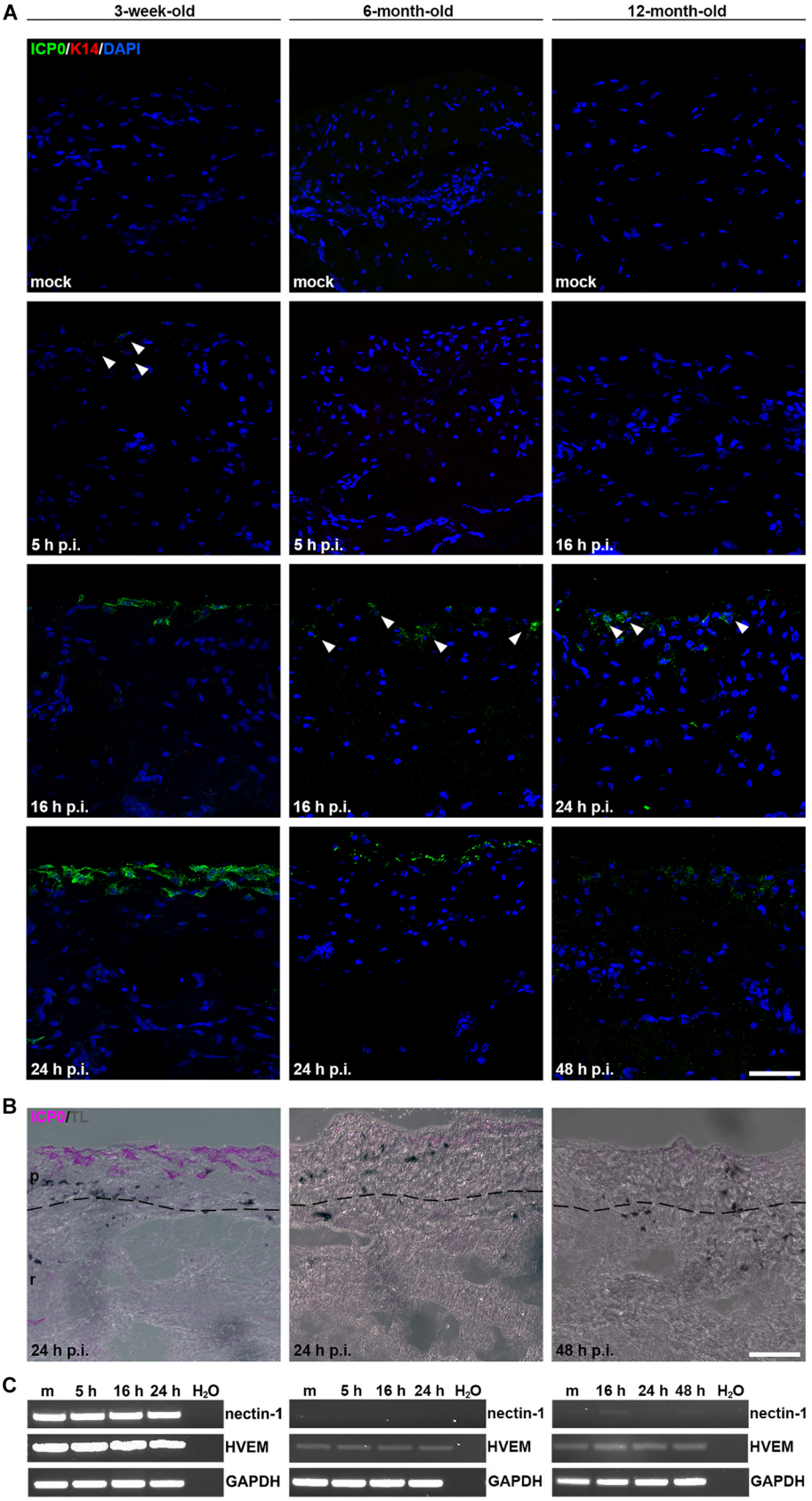

FIG 3 Infection efficiency of HSV-1 in the dermis from aging mice. (A) After infection of dermal sheets with HSV-1 at 50 PFU/cell, cross sections visualize ICP0-expressing cells (green) (arrowhead) in 3-week-old dermis

(Continued on next page)

percentages were previously found on murine primary dermal fibroblasts (14). These results indicate that the surface expression of HVEM varies with aging only to a minor extent. Whether the transcriptional activity of HVEM decreases during aging as suggested by RT-PCR was not followed.

When we analyzed cell surface expression of nectin-1, it was detected on ca. 40% of the analyzed cells from 3-week-old dermis (Fig. 5B). To address whether the varying expression level of nectin-1 in juvenile dermis is tissue dependent or an intrinsic feature of the fibroblasts, we isolated fibroblasts from 3-week-old dermis. After one passage in culture, flow cytometric analyses revealed nectin-1 on ca. 38% of the analyzed cells, again with some varying level of expression (Fig. 5C). Of note, infection efficiencies were comparable, and it was when nectin-1 was detected on just 6% of the cells that early infection was delayed (data not shown). These results imply that surface expression of nectin-1 varies in juvenile dermis as well as in young fibroblasts in culture, however, to a level that still allows comparable infection efficiency.

Strikingly, the mean percentage of nectin-1-expressing cells decreased to ca. 18 and 10% in 6- and 12- to 18-month-old dermis, respectively (Fig. 5B). Thus, we conclude that nectin-1 expression drops in the dermis during aging, while HVEM remains constantly detected. To compare receptor expression to infection efficiency during aging, we quantified ICP0 stainings in dermal sheets of young and aged mice. The analyses of 3-week- and 12-month-old dermis indicated a strong decrease of ICP0 stainings at 16 h p.i. in the aged dermis, which was less pronounced in the adult (6-month-old) dermis (Fig. 5D). As the detection of ICP0 in aged dermis at 48 h p.i. demonstrated a somehow comparable number of infected cells as in young and adult dermis at 24 h p.i. (Fig. 3A), we concluded that aged dermis was still susceptible to HSV-1, but infection efficiency was strongly delayed during aging. Previously, delayed infection onset was found in nectin-1-deficient dermal fibroblasts, suggesting that HVEM serves as a less efficient receptor (14). As the cell surface expression of HVEM was constantly high in young and aged dermis, we suggest that delayed infection efficiency in aged dermis correlates with less nectin-1 and thus increased usage of HVEM as a receptor.

Infection of nectin-1-deficient dermis of aged mice. To further support the correlation of nectin-1 expression and infection efficiency in aged dermis, we *ex vivo* infected dermal sheets from 12-month-old nectin-1-deficient mice. At 16 h p.i., no infection was visible, while some infected cells were detected at 24 h p.i., which was comparable to old dermis from wild-type (WT) mice (Fig. 3A and Fig. 6A). Yet we observed nearly no increase in the number of infected cells at 48 h p.i., which was in contrast to WT mice (Fig. 3A and Fig. 6A). Costaining with a macrophage marker excluded that the infected cells represented macrophages (Fig. 6A). When we investigated receptor expression, RT-PCR revealed no HVEM RNAs and confirmed the absence of nectin-1 (Fig. 6B). Surface expression of HVEM was found on ca. 41 and 5% of cells from 12-month- and 18-month-old nectin-1-deficient dermis, respectively, which was clearly lower than in the aged dermis from WT mice (Fig. 6C). These results suggest that in the absence of nectin-1, HSV-1 susceptibility in the aged dermis is not only delayed but also reduced compared to the aged dermis from WT mice because of low HVEM expression. In summary, the finding of the reduced infection in the absence of nectin-1 strengthens the correlation of nectin-1 and HVEM expression levels and infection efficiencies rather than mechanical changes in aged dermis.

FIG 3 Legend (Continued)
at 5 h p.i., in 6-month-old dermis at 16 h p.i., and in 12-month-old dermis at 24 h p.i. The number of ICP0-expressing cells strongly increases in 3-week- and 6-month-old dermis at 24 h p.i., whereas the increase was less pronounced in 12-month-old dermis at 48 h p.i. Confocal projections and merged images from at least 5 independent experiments are shown with DAPI (blue) as the nuclear counterstain and keratin 14 (red) as a control. Scale bar, 50 μm. (B) Transmission light indicates the morphology of the infected dermal sheets with no major cytopathic effects in the papillary dermis at late times. The estimated border of papillary (p) and reticular (r) dermis is marked by a dashed line. Scale bar, 50 μm. (C) RT-PCR ($n \geq 5$) revealed nectin-1 and HVEM transcripts during infection of the 3-week-old dermis. Nearly no nectin-1 and reduced HVEM signals were detected in 6- and 12-month-old dermis. m, mock infected.

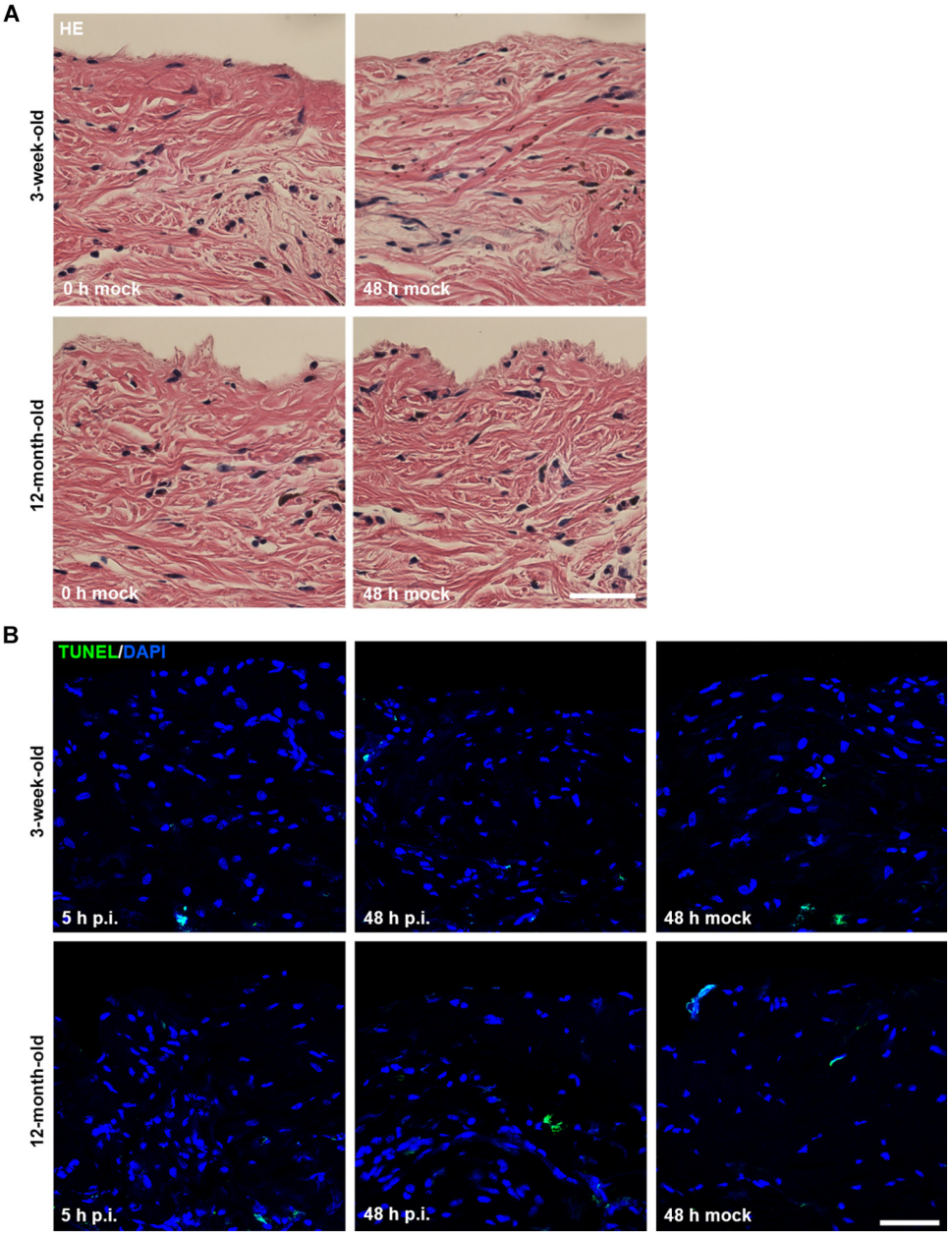

FIG 4 Structure and viability of juvenile and aged dermis. (A) Hematoxylin and eosin (H&E)-stained sections of mock-infected dermis from 3-week- and 12-month-old mice visualize the structural integrity prior to and after incubation in the medium for 48 h. Scale bar, 50 μm. (B) Confocal projections and merged images show single TUNEL-positive cells (green) with DAPI (blue) as the nuclear counterstain at 5 h p.i. as well as at 48 h p.i. and 48 h after incubation. Scale bar, 50 μm.

Infection efficiency and nectin-1 expression in the epidermis of aging mice. To address whether reduced nectin-1 expression and delayed infection during aging are restricted to the dermis, we also *ex vivo* infected epidermal sheets from young (3-week-old) and aged (12-month-old) mice at 50 PFU/cell. In both cases, epidermal whole mounts show ICP0 in cells of the basal keratinocyte layer by 3 h p.i., and nearly all cells expressed ICP0 at 6 h p.i. (Fig. 6E). In line with these results is our finding that expression of nectin-1 was comparable in young and aged epidermis (Fig. 6D). Taken together, we found no change in infection efficiency and nectin-1 expression in the epidermis during aging.

In contrast, in the absence of nectin-1, only very few infected cells were observed in aged epidermis (12 months old) at 6 h p.i. (Fig. 6E), which is a stronger decrease in the

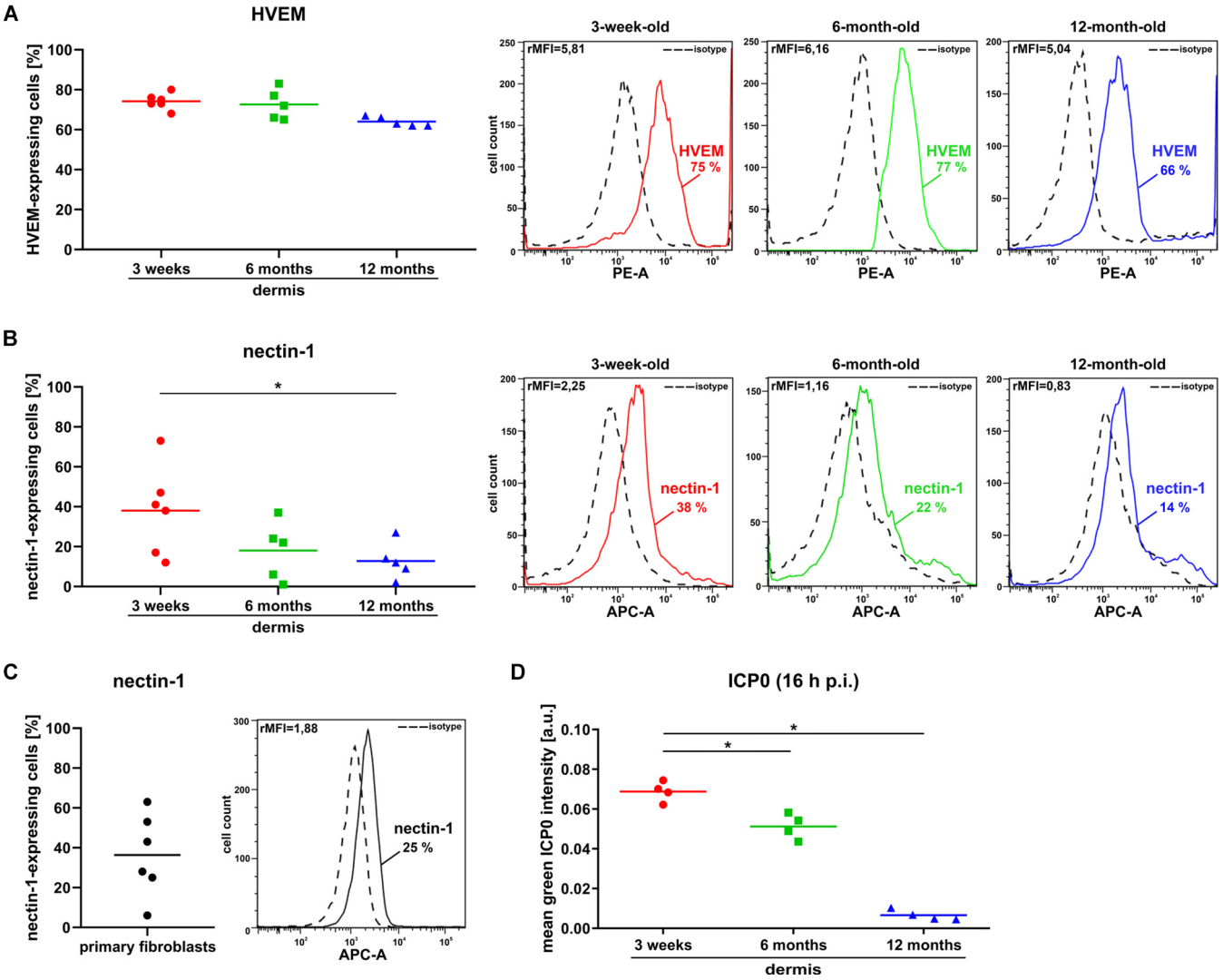

FIG 5 Comparison of receptor and ICP0 expression in dermis during aging. Cells were dissociated from dermal sheets of 3-week-, 6-month-, and 12-month-old mice by DMEM suspension buffer followed by staining surface expression of HVEM (A) or nectin-1(B). Flow cytometric analyses indicate a constantly high number of HVEM-expressing cells comparing young and aged dermis (A), whereas the number of nectin-1-expressing cells is in total lower and variable and decreases significantly during aging (B). (A, B) Results of 5 to 6 independent experiments are shown as dot blots. Representative profiles indicate the number of HVEM- or nectin-1-expressing cells and the relative median fluorescence intensities (rMFI). PE-A, phycoerythrin antibody; APC-A, allophycocyanin antibody. (C) Cells were dissociated from dermal sheets of 3-week-old mice by DMEM suspension buffer and kept in culture for one passage followed by flow cytometric analyses. The results of primary fibroblasts from 6 individual dermal sheets shown as dot blots demonstrate the variable number of nectin-1-expressing cells. A representative profile is shown. (D) Dermal sheets of 3-week-, 6-month-, and 12-month-old mice were infected with HSV-1 at 50 PFU/cell for 16 h. Infected cells were visualized by staining of ICP0, which was quantified in 4 independent experiments and is shown as a dot blot. The results indicate a significant decrease of ICP0 stainings during aging. *P* values of ≤ 0.05 (*) are shown.

number of infected cells than in nectin-1-deficient epidermis from newborn back skin and adult (1-month-old) tail skin (10). The finding of strongly decreased infection in the absence of nectin-1 might correlate with the undetectable surface expression of HVEM in aged epidermis (data not shown). In newborn mice, HVEM is present on the surface for at least a subpopulation of keratinocytes in the epidermis of WT and nectin-1-deficient mice (10). The restricted presence of HVEM in nectin-1-deficient epidermis can potentially replace nectin-1 as a receptor and thus allow a decreased but still detectable number of infected cells at 3 h p.i. (10).

In summary, our results suggest that the comparable early onset of infection in the epidermis of young and aged mice is related to the presence of nectin-1. However, when nectin-1 is absent, the undetectable HVEM expression in the aged epidermis might play a role in the strong decrease of infection efficiency.

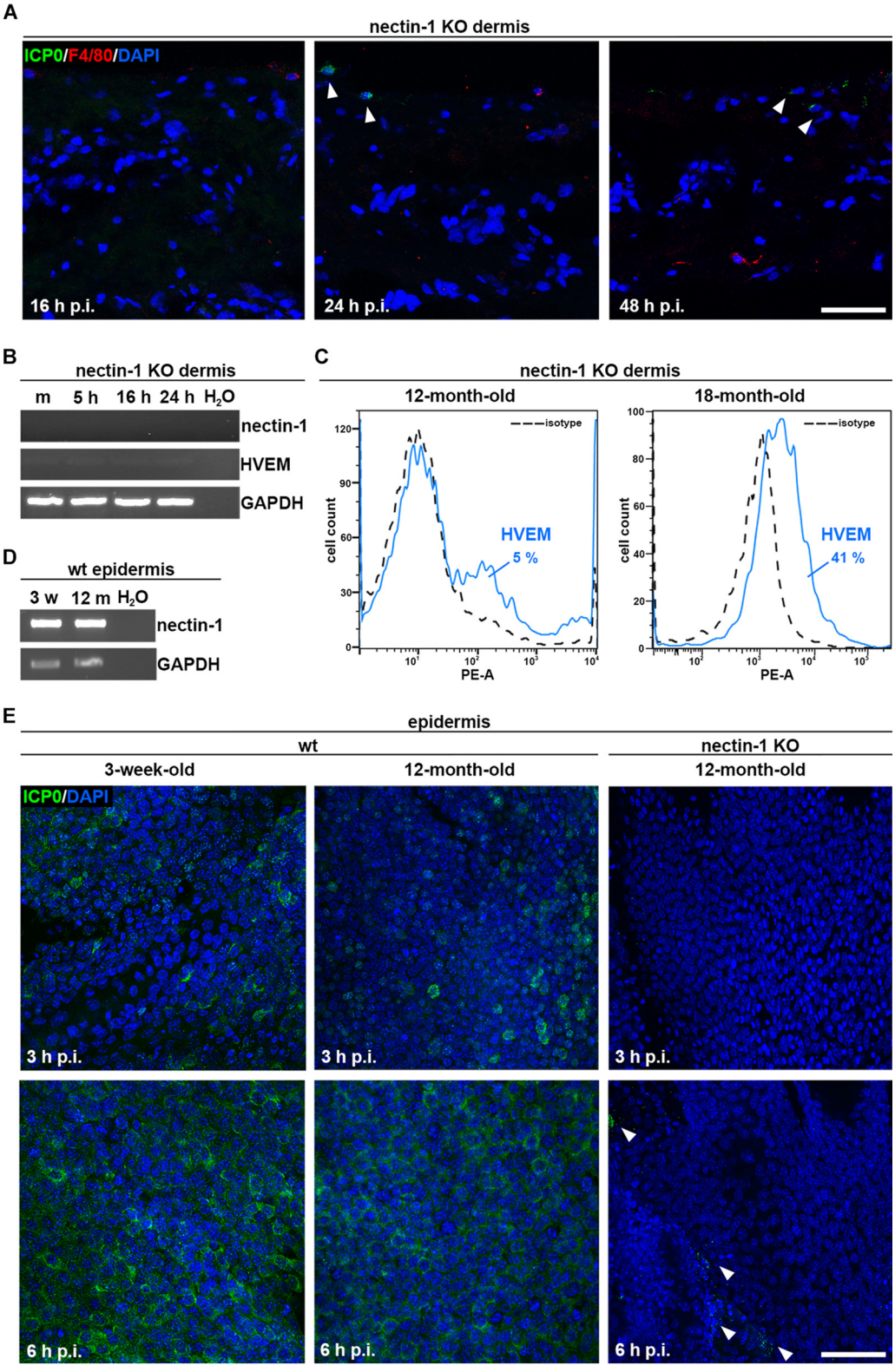

FIG 6 Infection efficiency of HSV-1 in nectin-1-deficient dermis and epidermis. (A) Dermal sheets of 12-month-old nectin-1 knockout (KO) mice were infected at 50 PFU/cell. Staining of ICP0 (green) in cross sections visualized few infected cells (arrowhead) at 24 h and 48 h p.i. Costaining with the macrophage marker F4/80 (red) revealed few macrophages which were not infected. Confocal projections and merged images show DAPI (blue) as the nuclear counterstain. Scale bar, 50 μm. (B) RT-PCR ($n = 1$) demonstrates no nectin-1 transcripts and minor signals for HVEM in the 12-month-old nectin-1-deficient dermis. Results are shown at various time points after infection. m, mock infected. (C) Cells were dissociated from dermal sheets of 12- and 18-month-old nectin-1 KO mice by DMEM suspension buffer. Flow cytometric

(Continued on next page)

Overall, the delayed infection efficiency and reduced surface expression of nectin-1 was only observed in the aged dermis but not in the epidermis of aging mice.

DISCUSSION

How HSV-1 successfully penetrates target tissues such as skin and mucosa to initiate infection is poorly understood. Previously, we focused on the epidermis and the epithelium to identify skin barrier functions that interfere with the accessibility of cellular receptors (8, 10, 25, 26). Here, we addressed the susceptibility of murine dermis to HSV-1. As age-related skin alterations are most evident in the dermis, we explored whether aging of this tissue contributes to the availability and accessibility of the receptors nectin-1 and HVEM. A hallmark of aging skin is the unbalanced homeostasis of the dermal extracellular matrix, which comprises the bulk of the skin. During aging, collagen I, the most abundant structural protein in the dermis, undergoes organizational and structural changes which impact the behavior of fibroblasts, leading to altered morphology, spreading, mechanical force, and communication with the ECM (27).

As dermal fibroblasts in culture are highly susceptible to HSV-1, we wondered whether, in principle, the fibroblast-ECM interactions contribute to alterations in the accessibility of cells, which may influence infection efficiencies. Our *ex vivo* infection assays demonstrate that HSV-1 can penetrate into murine dermis once the epidermis is removed; however, there was a major delay of the detectable onset of infection compared to fibroblasts in culture. To address whether the ECM acts as a potential barrier for viral invasion, we infected fibroblasts embedded in collagen matrices. With increasing collagen concentrations, we observed a delayed onset of infection from 3 to 6 h p.i., supporting that the collagen matrix contributes to delayed infection efficiency. To follow up this assumption, we infected dermal sheets prepared from embryonic (E14.5) skin, for which the ECM is not yet fully mature, and observed viral transcripts already at 3 h p.i. (data not shown). At 3 h p.i., we also detected viral transcripts in the newborn dermis; however, this finding is most likely related to the infection of hair follicle-associated keratinocytes, which are still present in the dermal sheets of newborns but not in the embryonic dermal sheets. Taken together, we conclude that the ECM provides a barrier that does not prevent but rather delays access to the fibroblasts. As fibroblasts embedded in the dermis or in collagen matrices are under mechanical stress, we cannot exclude that the cellular stress responses also play a role in viral susceptibility.

Strikingly, infection efficiency of the dermis decreased during aging. As the transcriptome of dermal fibroblasts changes during aging at least in human dermis (28), we explored potential changes of receptor expression in the aged dermis. While the high surface expression of HVEM was unchanged during aging, the number of nectin-1-expressing cells was reduced from ca. 40% to 10% in aged (12-month-old) dermis. Cell spreading and cell surface attachment of the fibroblasts to the fragmented collagen fibrils can be strongly reduced, as observed in aged human dermis (29). Thus, the decreased nectin-1 expression might be a response to the age-related changes of cell adhesion and cellular morphology, although in another tissue, the age-dependent reduction of nectin-1 expression has also been observed in the mouse brain (30).

Our results suggest that the reduced availability of nectin-1 leads to an increased usage of HVEM as the receptor in the aged dermis. This assumption is based on our recent infection studies of murine dermal fibroblasts which demonstrate slower virus

FIG 6 Legend (Continued)
analyses indicate 5% and 41% of cells were positive for HVEM. PE-A, phycoerythrin antibody. (D) RT-PCR ($n = 3$) demonstrates nectin-1 transcripts in 3-week- (3w) and 12-month-old (12m) WT epidermis. (E) Epidermal sheets from WT and nectin-1 KO mice were infected with HSV-1 at 50 PFU/cell. Immunostainings of whole mounts show comparable numbers of ICP0-expressing cells (green) in the basal keratinocyte layer of 3-week- and 12-month-old WT mice at 3 h and 6 h p.i. In contrast, very few infected cells (arrowhead) were found in 12-month-old dermis in the absence of nectin-1 at 6 h p.i. Scale bar, 50 μm.

entry in the absence of nectin-1 (14). Thus, we assume that the delayed onset of infection in aged dermis is based on HVEM acting as a less efficient receptor. In addition, the age-dependent alterations of the ECM and the corresponding cellular responses might influence infection efficiency. In the aged nectin-1-deficient dermis, only a few cells were infected, even after longer infection times, and HVEM expression was strongly reduced. These observations argue that it is the availability rather than the accessibility of the receptors nectin-1 and HVEM that most likely determine infection efficiency in the aged dermis.

In contrast to the delayed infection and the reduced nectin-1 expression in the aged dermis, we found comparable infection efficiencies in epidermal sheets from young and aged (12-month-old) mice. As expected, the level of nectin-1 did not change in the epidermis during aging, supporting that the availability of nectin-1 is a key contributor to infection efficiency. Our recent studies in the nectin-1-deficient epidermis demonstrated a strongly reduced infection, indicating that nectin-1 serves as the major receptor in the basal keratinocyte layer of the epidermis (10). In the absence and presence of nectin-1, HVEM is present on a limited number of keratinocytes in the epidermis, which led us to conclude that HVEM acts as an alternative receptor in the absence of nectin-1, causing a rather limited and slower infection (10). In line with this conclusion is our observation that in aged nectin-1-deficient epidermis, no surface expression of HVEM was detected, and thus, cells were rarely infected.

Overall, our *ex vivo* infection studies demonstrated that the murine dermis is susceptible to HSV-1; however, the onset of infection is strongly delayed and less efficient, not only compared to fibroblasts in culture but also to epidermal sheets. Thus, we assume that the ECM delays viral access to the major receptor nectin-1. Age-related changes of the ECM and its interactions with the dermal fibroblasts do not enhance accessibility of the cells, but rather, delayed infection efficiency was observed. As the surface expression of nectin-1 declines in the aged dermis, we conclude that the reduced receptor availability contributes to the delay in infection. The challenge of future experiments is to explore how the ECM serves as a barrier for the penetration of HSV-1 and whether age-dependent alterations enhance the delayed infection efficiency in addition to the reduced availability of nectin-1 as a receptor.

MATERIALS AND METHODS

Preparation of murine skin and isolation of dermal fibroblasts. Murine skin samples were taken from the backs of newborn mice (C57BL/6), from the tails of juvenile (3-week-old), adult (6-month-old), and aged (12-month-old) mice (C57BL/6), and from the tails of 12- and 18-month-old Pvrl$^{-/-}$ mice (10), referred to as nectin-1-deficient mice throughout the text. Breeding problems made dermis from young Pvrl$^{-/-}$ mice (C57BL/6) unavailable. Murine epidermal sheets taken from the tail skin of WT and nectin-1-deficient mice were prepared by the removal of the dermis by dispase II treatment and processed as described previously (9, 10). Dermal sheets were taken from back skin (newborn) and tail skin (juvenile to aged). After incubation for 30 to 45 min at 37°C with 4 U/ml dispase II (Roche) in phosphate-buffered saline (PBS), the dermis was gently separated from the epidermis with forceps. Dermal and epidermal sheets were incubated in Dulbecco modified Eagle medium (DMEM)-high glucose-GlutaMAX (Life Technologies) containing 10% fetal calf serum (FCS), penicillin (100 IU/ml), and streptomycin (100 μg/ml).

Primary fibroblasts were isolated from newborn or juvenile (3-week-old) dermis after shaking gently for 60 min in a DMEM suspension buffer containing 400 U/ml collagenase I, 200 U/ml collagenase IV, 400 U/ml hyaluronidase IV-S, 0.05% DNase I, and penicillin (100 IU/ml)/streptomycin (100 μg/ml). After isolation, primary fibroblasts were maintained in DMEM-high glucose-GlutaMAX containing 10% FCS, penicillin (100 IU/ml), and streptomycin (100 μg/ml), and experiments were performed at passages 2 to 3 after isolation.

Collagen matrices. Primary murine fibroblasts isolated from newborn mice were embedded in floating collagen I lattices (20). In brief, the lattice solution was prepared by adding rat tail collagen I (Corning) to DMEM buffered by the addition of 0.1 M NaOH and FCS followed by the supply of 1×10^6 fibroblasts/gel. The lattice solution was dispensed into uncoated 6-cm dishes and incubated at 37°C. Floating gels detached after 1 to 2 h of polymerization.

Virus. Infection studies were performed with purified preparations of HSV-1 WT strain 17 as described (31). Virus inoculum was added to epidermal or dermal sheets or to cells at 37°C, and the defining time point was zero. For infection of epidermal and dermal sheets, the calculation of the virus dose was

based on the estimated number of cells in the basal layer of the epidermis (ca. 2×10^5 cells per 5- by 5-mm sheet) and in the superficial areas of the dermis (3×10^5 per 3- by 3-mm sheet), respectively. Skin samples were infected at 50 PFU/cell and primary fibroblasts at 5 PFU/cell. Epidermal sheets were floating on a virus-containing medium, while dermal sheets were submerged. The virus inoculum was replaced by the medium at 1 h p.i. Floating collagen matrices were infected at 50 PFU/cell by floating on a virus-containing medium.

Ethics statement. The preparation of skin and dermal cells from sacrificed animals was carried out in strict accordance with the recommendations of the Guide of Landesamt für Natur, Umwelt und Verbraucherschutz, Northrhine-Westphalia (LANUV NRW) (Germany). The study was approved by LANUV NRW.

RNA preparation and RT-PCR. RNA was isolated from cells or tissue by use of Nucleozol reagents (Macherey-Nagel). cDNA was synthesized using the SuperScript II reverse transcriptase (Life Technologies), and PCR was performed with *Taq* DNA polymerase (Life Technologies). The nectin-1 primers (forward, 5′-GTCCTGGGAAACACGGCTAA-3′, and reverse, 5′-TAGGTCCCCGGAAGAAGAGG-3′) generated a 368-bp fragment, the HVEM primers (forward, 5′-CCACTGTTCCACATGCTTGC-3′, and reverse, 5′-GCTG TTGGTCCCACGTCTTA-3′), a 196-bp fragment; the ICP0 primers (forward, 5′-ATGTCTGGGTGTTTCCCTGC-3′, and reverse, 5′-TCTCGAACAGTTCCGTGTCC-3′), a 147-bp fragment; the gD primers (forward, 5′-CCC GCTACCGACTTATCGAC-3′, and reverse, 5′-CCCGCTACCGACTTATCGAC-3′), a 368-bp fragment; the keratin 5 primers (forward, 5′-TCGAAACACCAAGCACGAGA-3′, and reverse, 5′-CTTCAGCAATGGCGTTCT GG-3′), a 113-bp fragment; and the GAPDH (glyceraldehyde-3-phosphate dehydrogenase) primers (forward, 5′-TGATGACATCAAGAAGGTGGTGAAG-3′, and reverse: 5′-TCCTTGGAGGCCATGTGGGCCAT-3′), a 240-bp fragment.

Immunocytochemistry and antibodies. For whole mounts (17, 32), murine epidermal sheets were fixed with 3.4% formaldehyde for 2 h, stained overnight with mouse anti-ICP0 (monoclonal antibody 11060; 1:60) (33), and visualized with the corresponding secondary antibody and DAPI (4′,6-diamidino-2-phenylindole) as a nuclear counterstain as described (9).

For cryosections and horizontal whole mounts, murine dermal sheets were embedded in OCT compound (Sakura) in peel-off molds, frozen in liquid nitrogen, and cut with the cryomicrotome CM3050S (Leica) at −24°C into 100-μm cross sections or horizontal whole mounts to preserve the integrity of the tissue as described (34) (Fig. 1A). After direct transfer into PBS to dissolve OCT, the samples were fixed with 3.4% formaldehyde for 2 h and incubated in dermis-blocking buffer containing 0.5% skim milk powder, 0.25% gelatin from cold-water fish skin, 0.5% Triton X-100, 0.5% NGS (normal goat serum), and 0.1% BSA (bovine serum albumin) in TBS (Tris-buffered saline) for 4 h, all at room temperature. For immunofluorescence, whole mounts and cross sections were costained with mouse anti-ICP0 (catalog no. 11060; 1:60) (33), and rabbit anti-keratin 14 (1:8000) (Covance) overnight at 4°C followed by incubation with the corresponding secondary antibodies and DAPI. After fixation, cross sections of nectin-1-deficient dermis were incubated in dermis-blocking buffer without Triton X-100 for 4 h at room temperature and were stained with rat anti-F4/80 (BM8; 1:200) (Dianova) overnight at 4°C followed by the corresponding secondary antibody. Subsequently, sections were incubated for 2 h in dermis-blocking buffer and stained with mouse anti-ICP0 (1:60) overnight at 4°C followed by the corresponding secondary antibodies and DAPI. For H&E staining, paraffin-embedded 8-μm tissue sections were stained for 10 min with hemalum to visualize nuclei followed by counterstaining of the cytoplasm with eosin for 30 s. For detection of DNA fragmentation, paraffin-embedded tissue sections were permeabilized with proteinase K (20 μg/ml) for 8 min at room temperature and fixed with 4% formaldehyde (methanol free), labeled using the DeadEnd fluorometric TUNEL system (Promega), and counterstained with DAPI for 4 min.

Microscopy was performed using a Leica DM IRB/E microscope linked to a Leica TCS-SP/5 confocal unit. Images were assembled by use of Photoshop Elements 2018. Images were analyzed by use of FiJi (version 2.0.0-rc-65/1.51s) (35) by measuring the mean green fluorescent intensity of three different areas per biological replicate.

Flow cytometric analysis. Murine primary fibroblasts from WT mice were detached with 0.05% trypsin-0.02% EDTA for staining with mouse anti-nectin-1 (CK41; 1:100) (36). Dermal sheets from WT or nectin-1-deficient mice were digested with DMEM suspension buffer containing 400 U/ml collagenase I, 200 U/ml collagenase IV, 400 U/ml hyaluronidase IV-S, 0.05% DNase I, and penicillin (100 IU/ml)/streptomycin (100 μg/ml) and shaken gently for 60 min at 37°C. Cell suspensions were filtered through cell strainers (40 μm; Falcon) and incubated in PBS/5% FCS on ice for 30 min with mouse anti-nectin-1 (CK41; 1:100) or with Armenian hamster anti-HVEM (clone HMHV-1B18; BioLegend; 1:200). Nectin-1 was visualized with anti-mouse IgG-Cy5 (Jackson Immunoresearch Laboratories Inc.; 1:100), and HVEM was visualized with anti-hamster IgG-PE (eBioscience; 1:50). For nectin-1, mouse IgG1 (Life Technologies; 1:20), and for HVEM Armenian hamster, IgG (eBioscience; 1:50) were used as isotype controls. Previous controls showed the specificity of the anti-nectin-1 antibody CK41 (36) and of the anti-HVEM antibody in nectin-1-deficient and HVEM-deficient fibroblasts, respectively (14). Samples were stained with DAPI 1 min prior to analysis, which allowed the gating of only viable cells. Samples were analyzed by using a fluorescence-activated cell sorter (FACS)Canto II flow cytometer and FACSDiva (version 6.1.3; BD) and FlowJo (version 7.6.3, Tree Star) software. Median fluorescent intensity (MFI) of flow cytometry analyses was calculated using FlowJo software. Relative MFI was calculated by the formula $\frac{(\mathrm{MFI}_{\mathrm{staining}} - \mathrm{MFI}_{\mathrm{isotype}})}{\mathrm{MFI}_{\mathrm{isotype}}}$.

Statistics. For the statistical analyses, Student's *t* tests were performed to calculate *P* values using the unpaired two-tailed method. Differences were considered to be statistically significant with *P* values of ≤ 0.05.

ACKNOWLEDGMENTS

We are grateful to Hisham Bazzi for help with the embryonic skin. We thank Beate Eckes and Gabriele Scherr for discussions and help with the collagen matrices, Roger Everett for the antibodies against ICP0, Claude Krummenacher for the antibody against nectin-1 (CK41), and Bent Brachvogel and Paola Zigrino for comments on the manuscript.

This research was supported by the German Research Foundation (KN536/16-3 to D.K.-M. and SFB829 stipend to L.W.) the Köln Fortune Program/Faculty of Medicine, the University of Cologne, and the Maria-Pesch Foundation.

REFERENCES

1. Heldwein EE, Krummenacher C. 2008. Entry of herpesviruses into mammalian cells. Cell Mol Life Sci 65:1653–1668. https://doi.org/10.1007/s00018-008-7570-z.
2. Shukla D, Spear PG. 2001. Herpesviruses and heparan sulfate: an intimate relationship in aid of viral entry. J Clin Invest 108:503–510. https://doi.org/10.1172/JCI200113799.
3. Spear PG. 2004. Herpes simplex virus: receptors and ligands for cell entry. Cell Microbiol 6:401–410. https://doi.org/10.1111/j.1462-5822.2004.00389.x.
4. Connolly SA, Jackson JO, Jardetzky TS, Longnecker R. 2011. Fusing structure and function: a structural view of the herpesvirus entry machinery. Nat Rev Microbiol 9:369–381. https://doi.org/10.1038/nrmicro2548.
5. Eisenberg RJ, Atanasiu D, Cairns TM, Gallagher JR, Krummenacher C, Cohen GH. 2012. Herpes virus fusion and entry: a story with many characters. Viruses 4:800–832. https://doi.org/10.3390/v4050800.
6. Montgomery RI, Warner MS, Lum BJ, Spear PG. 1996. Herpes simplex virus-1 entry into cells mediated by a novel member of the TNF/NGF receptor family. Cell 87:427–436. https://doi.org/10.1016/S0092-8674(00)81363-X.
7. Geraghty RJ, Krummenacher C, Cohen GH, Eisenberg RJ, Spear PG. 1998. Entry of alphaherpesviruses mediated by poliovirus receptor-related protein 1 and poliovirus receptor. Science 280:1618–1620. https://doi.org/10.1126/science.280.5369.1618.
8. Rahn E, Petermann P, Thier K, Bloch W, Morgner J, Wickström SA, Knebel-Mörsdorf D. 2015. Invasion of herpes simplex virus type 1 into murine epidermis: an ex vivo infection study. J Invest Dermatol 135:3009–3016. https://doi.org/10.1038/jid.2015.290.
9. Rahn E, Thier K, Petermann P, Knebel-Mörsdorf D. 2015. Ex vivo infection of murine epidermis with herpes simplex virus type 1. J Vis Exp 102:e53046. https://doi.org/10.3791/53046.
10. Petermann P, Thier K, Rahn E, Rixon FJ, Bloch W, Özcelik S, Krummenacher C, Barron MJ, Dixon MJ, Scheu S, Pfeffer K, Knebel-Mörsdorf D. 2015. Entry mechanisms of herpes simplex virus 1 into murine epidermis: involvement of nectin-1 and herpesvirus entry mediator as cellular receptors. J Virol 89:262–274. https://doi.org/10.1128/JVI.02917-14.
11. Edwards RG, Kopp SJ, Karaba AH, Wilcox DR, Longnecker R. 2015. Herpesvirus entry mediator on radiation-resistant cell lineages promotes ocular herpes simplex virus 1 pathogenesis in an entry-independent manner. mBio 20:e01532-15. https://doi.org/10.1128/mBio.01532-15.
12. Edwards RG, Longnecker R. 2017. Herpesvirus entry mediator and ocular herpesvirus infection: more than meets the eye. J Virol 91:e00115-17. https://doi.org/10.1128/JVI.00115-17.
13. Shenoy R, Mostow E, Cain G. 2015. Eczema herpeticum in a wrestler. Clin J Sport Med 25:e18–e19. https://doi.org/10.1097/JSM.0000000000000097.
14. Petermann P, Rahn E, Thier K, Hsu MJ, Rixon FJ, Kopp SJ, Knebel-Mörsdorf D. 2015. Role of nectin-1 and herpesvirus entry mediator as cellular receptors for herpes simplex virus 1 on primary murine dermal fibroblasts. J Virol 89:9407–9416. https://doi.org/10.1128/JVI.01415-15.
15. Sorrell JM, Caplan AI. 2004. Fibroblast heterogeneity: more than skin deep. J Cell Sci 117:667–675. https://doi.org/10.1242/jcs.01005.
16. Driskell RR, Lichtenberger BM, Hoste E, Kretzschmar K, Simons BD, Charalambous M, Ferron SR, Herault Y, Pavlovic G, Ferguson-Smith AC, Watt FM. 2013. Distinct fibroblast lineages determine dermal architecture in skin development and repair. Nature 504:277–281. https://doi.org/10.1038/nature12783.
17. Petermann P, Haase I, Knebel-Mörsdorf D. 2009. Impact of Rac1 and Cdc42 signaling during early herpes simplex virus type 1 infection of keratinocytes. J Virol 83:9759–9772. https://doi.org/10.1128/JVI.00835-09.
18. Boutell C, Everett RD. 2013. Regulation of alphaherpesvirus infections by the ICP0 family of proteins. J Gen Virol 94:465–481. https://doi.org/10.1099/vir.0.048900-0.
19. Kessler D, Dethlefsen S, Haase I, Plomann M, Hirche F, Krieg T, Eckes B. 2001. Fibroblasts in mechanically stressed collagen lattices assume a "synthetic" phenotype. J Biol Chem 276:36575–36585. https://doi.org/10.1074/jbc.M101602200.
20. Eckes B, Wang F, Rittié L, Scherr G, Zigrino P. 2017. Cell-populated collagen lattice models. Methods Mol Biol 1627:223–233. https://doi.org/10.1007/978-1-4939-7113-8_15.
21. Grinnell F, Petroll WM. 2010. Cell motility and mechanics in three-dimensional collagen matrices. Annu Rev Cell Dev Biol 26:335–361. https://doi.org/10.1146/annurev.cellbio.042308.113318.
22. Daly CH, Odland GF. 1979. Age-related changes in the mechanical properties of human skin. J Invest Dermatol 73:84–87. https://doi.org/10.1111/1523-1747.ep12532770.
23. Lavker RM, Zheng PS, Dong G. 1987. Aged skin: a study by light, transmission electron, and scanning electron microscopy. J Invest Dermatol 88:44s–51s. https://doi.org/10.1038/jid.1987.9.
24. Jenkins G. 2002. Molecular mechanisms of skin aging. Mech Ageing Dev 123:801–810. https://doi.org/10.1016/s0047-6374(01)00425-0.
25. Rahn E, Thier K, Petermann P, Rübsam M, Staeheli P, Iden S, Niessen CM, Knebel-Mörsdorf D. 2017. Epithelial barriers in murine skin during herpes simplex virus 1 infection: the role of tight junction formation. J Invest Dermatol 137:884–893. https://doi.org/10.1016/j.jid.2016.11.027.
26. Thier K, Petermann P, Rahn E, Rothamel D, Bloch W, Knebel-Mörsdorf D. 2017. Mechanical barriers restrict invasion of herpes simplex virus 1 into human oral mucosa. J Virol 91:e01295-17. https://doi.org/10.1128/JVI.01295-17.
27. Cole MA, Quan T, Voorhees JJ, Fisher GJ. 2018. Extracellular matrix regulation of fibroblast function: redefining our perspective on skin aging. J Cell Commun Signal 12:35–43. https://doi.org/10.1007/s12079-018-0459-1.
28. Tigges J, Krutmann J, Fritsche E, Haendeler J, Schaal H, Fischer JW, Kalfalah F, Reinke H, Reifenberger G, Stühler K, Ventura N, Gundermann S, Boukamp P, Boege F. 2014. The hallmarks of fibroblast ageing. Mech Ageing Dev 138:26–44. https://doi.org/10.1016/j.mad.2014.03.004.
29. Varani J, Dame MK, Rittie L, Fligiel SE, Kang S, Fisher GJ, Voorhees JJ. 2006. Decreased collagen production in chronologically aged skin: roles of age-dependent alteration in fibroblast function and defective mechanical stimulation. Am J Pathol 168:1861–1868. https://doi.org/10.2353/ajpath.2006.051302.
30. Shiotani H, Maruo T, Sakakibara S, Miyata M, Mandai K, Mochizuki H, Takai Y. 2017. Aging-dependent expression of synapse-related proteins in the mouse brain. Genes Cells 22:472–484. https://doi.org/10.1111/gtc.12489.
31. Schelhaas M, Jansen M, Haase I, Knebel-Mörsdorf D. 2003. Herpes simplex virus type 1 exhibits a tropism for basal entry in polarized epithelial cells. J Gen Virol 84:2473–2484. https://doi.org/10.1099/vir.0.19226-0.
32. Braun KM, Niemann C, Jensen UB, Sundberg JP, Silva-Vargas V, Watt FM. 2003. Manipulation of stem cell proliferation and lineage commitment: visualisation of label-retaining cells in wholemounts of mouse epidermis. Development 130:5241–5255. https://doi.org/10.1242/dev.00703.
33. Everett RD, Cross A, Orr A. 1993. A truncated form of herpes simplex

virus type 1 immediate-early protein Vmw110 is expressed in a cell type dependent manner. Virology 197:751–756. https://doi.org/10.1006/viro.1993.1651.
34. Salz L, Driskell RR. 2017. Horizontal whole mount: a novel processing and imaging protocol for thick, three-dimensional tissue cross-sections of skin. J Vis Exp 126:56106. https://doi.org/10.3791/56106.
35. Schindelin J, Arganda-Carreras I, Frise E, Kaynig V, Longair M, Pietzsch T, Preibisch S, Rueden C, Saalfeld S, Schmid B, Tinevez JY, White DJ, Hartenstein V, Eliceiri K, Tomancak P, Cardona A. 2012. Fiji: an open-source platform for biological-image analysis. Nat Methods 9:676–682. https://doi.org/10.1038/nmeth.2019.
36. Krummenacher C, Baribaud I, Ponce de Leon M, Whitbeck JC, Lou H, Cohen GH, Eisenberg RJ. 2000. Localization of a binding site for herpes simplex virus glycoprotein D on herpesvirus entry mediator C by using antireceptor monoclonal antibodies. J Virol 74:10863–10872. https://doi.org/10.1128/jvi.74.23.10863-10872.2000.